Analytical model for the prediction of the tensile behaviour of corroded steel bars

Zeng, Chaoqun; Zhu, Ji Hua; Xiong, Cheng; Li, Yanru; Li, Dawang; Walraven, Joost

DOI
10.1016/j.conbuildmat.2020.120290

Publication date
2020

Document Version
Final published version

Published in
Construction and Building Materials

Construction and Building Materials 258 (2020) 120290

Contents lists available at ScienceDirect

Construction and Building Materials

journal homepage: www.elsevier.com/locate/conbuildmat

Analytical model for the prediction of the tensile behaviour of corroded steel bars

Chaoqun Zeng [a,b], Ji-Hua Zhu [a,b,*], Cheng Xiong [a,b], Yanru Li [a,b], Dawang Li [a,b], Joost Walraven [c]

[a] Guangdong Province Key Laboratory of Durability for Marine Civil Engineering, School of Civil Engineering, Shenzhen University, Shenzhen, Guangdong 518060, PR China
[b] College of Civil and Transportation Engineering, Shenzhen University, Shenzhen 518060, PR China
[c] Faculty of Civil Engineering and Geosciences, Dept. of Structural Engineering, Delft Univ. of Technology, Stevinweg 1, 2628 CN Delft, Netherlands

HIGHLIGHTS

- An analytical model was developed to predict the tensile behaviour of the corroded steel bars.
- The proposed model was validated using slotted steel bars and electrochemically corroded steel bars.
- Yield strength, ultimate strength and ductility of the corroded steel bars were predicted using the proposed model.

ARTICLE INFO

Article history:
Received 14 February 2020
Received in revised form 28 April 2020
Accepted 16 July 2020

Keywords:
Steel bar corrosion
Analytical model
Tensile strength
Ductility

ABSTRACT

An analytical model was developed to predict the tensile behaviour of a corroded steel bar. The model was established based on cross sectional analysis and was validated using experimental data for slotted steel bars and electrochemically corroded steel bars. The model was further used to predict the tensile behaviour of a corroded steel bar. The corrosion mode of the steel bar was supposed to be pitting corrosion and the distribution of the corroded section was supposed to follow a lognormal distribution. A power law between the parameters of the lognormal distribution and the average corrosion rate of the steel bar was used to predict the statistical distribution of the cross section area of a corroded steel bar. Based on these assumptions, the yield strength, ultimate strength and ductility of a corroded steel bar were predicted with different corrosion rates. The predicted behaviours are compared to collected experimental results from various sources. It is found that the numerical results of yield strength and ultimate strength agree well with the collected experimental results. The model slightly underestimates the ductility of the corroded steel bars. The result of the model would be helpful for the prediction of the tensile behaviour of reinforced concrete member subjected to chloride induced corrosion.

1. Introduction

The corrosion of steel bars induced by chloride ions is a critical issue for the structural safety of reinforced concrete structures exposed to high-chloride environments [1–8]. Corrosion of steel bars can lead to a reduction in the cross-sectional area, thereby reducing the bearing capacity of the structural members [1–6]. To maintain the performance and safety of reinforced concrete structures, various methods exist for detecting the corrosion of steel bars [9–15]. Steady-state polarisation response techniques are commonly used to predict the corrosion rate of steel bars inside reinforced concrete [8–12]. The recent development of inspection techniques such as 3D optical scanning and X-ray tomography allows scanning of the 3D profiles of corroded steel bars with higher accuracy [14–19]. These advanced detection methods allow the development of a probabilistic model of a corroded section [17–21].

The most common form of steel corrosion for reinforced concrete structures exposed to high-chloride environments is pitting corrosion [16–21]. Pitting corrosion causes localised corrosion at a point or small area, thus greatly reducing the cross-section area of the corroded steel bars. For the purpose of characterising pitting corrosion, several researchers have conducted experiments on prestressing wires and steel pipelines. The time and spatial variability of the maximum pitting depth of corroded reinforcing bars were obtained [19–22]. These studies proposed time-variant probabilis-

* Corresponding author at: Guangdong Province Key Laboratory of Durability for Marine Civil Engineering, School of Civil Engineering, Shenzhen University, Shenzhen, Guangdong 518060, PR China.
E-mail addresses: chaoqun.zeng@szu.edu.cn (C. Zeng), zhujh@szu.edu.cn (J.-H. Zhu), xiongcheng@szu.edu.cn (C. Xiong), liyanru@szu.edu.cn (Y. Li), dawangli163@163.com (D. Li), J.C.Walraven@tudelft.nl (J. Walraven).

https://doi.org/10.1016/j.conbuildmat.2020.120290
0950-0618/

Nomenclature

F	Tensile force	σ_y	Relative yield stress of the corroded steel bar
σ	Average stress	F_y	Yield load of the corroded steel bar
s	Surface area	F_{y0}	Yield load of the uncorroded steel bar
x	Longitudinal coordinate	σ_u	Relative ultimate strength of the corroded steel bar
ε	Average strain	F_u	Ultimate load of the corroded steel bar
L	Length of the steel bar	F_{u0}	Ultimate load of the uncorroded steel bar
ζ	Function linking the strain to the stress of the material	ε_u	The ductility of the corroded steel bar
φ	Inverse function ofζ	ΔL_f	Elongation of the corroded steel bar at maximum force
μ and m	Parameters of the log-normal distribution	ΔL_{f0}	Elongation of the uncorroded steel bar at maximum force
w	Average corrosion rate by mass loss		

tic distribution models of the maximum pitting depth [18–25]. Using a 3D scanning method, Kashani et al. [19] demonstrated that the pitted section follows log-normal distribution models. The shape parameters of the log-normal distribution can be determined by the mass loss ratio. These results greatly improve our knowledge about the time and spatial dependency of pitting corrosion on the surface of steel bars.

At present, the tensile behaviour of corroded steel bars at different corrosion levels is mainly predicted by empirical models based on experimental data [1–7]. Examples include corrosion tests of reinforcing steel bars taken from reinforced concrete exposed to natural [1–3] or to marine environments [4–6] and laboratory accelerated corrosion tests of steel bars embedded in concrete specimens under the action of an externally applied electric field [7–9]. Francois et al. [28] performed tensile test on steel bars embedded in 27-year-old corroded reinforced concrete beams and found that, when the average loss of mass on the whole corroded bar is used in the calculations, the elastic modulus is not influenced by the corrosion level. These findings suggest that the material properties of the steel bar are unaffected by corrosion. Recently, Li et al. [26] proposed a simplified constitutive model that allows the prediction of the tensile behaviour of corroded steel bars based on sectional analysis. Compared to a 3D finite element method, the proposed analytical model has several advantages. First, it can easily be implemented numerically and requires much less computation time. Second, the proposed analytical model allows the prediction of a corroded steel bar using a statistical model, even when the exact shape of the corroded steel bar is unknown, and this is seemingly impossible for 3D finite element software [27]. However, the proposed model used a bilinear model to simplify the stress–strain relationship, and the accuracy of the model was not satisfactory.

This paper proposed a significant improvement of the bilinear model using a more realistic shape function of the stress–strain curve. The proposed model was based on the assumption that the remaining material of the steel bar is unaffected by the corrosion product [5,26]. The effect of corrosion on reinforcement can be treated as only the cross-section reduction with no material degradation [26]. Based on these assumptions, a novel analytical model was developed using sectional analysis. A program written in *MATLAB* was proposed to numerically compute the elongation-load relationship of the corroded steel bar based on the uncorroded material properties. The proposed model was validated by comparing the numerical results to experimental results of slotted steel bars and electrochemically corroded steel bars. Three hundred corroded steel bars were generated numerically using the log-normal distribution of the corroded section. The load–displacement curves of the numerically generated steel bars were computed using the proposed analytical model. Relationships between the corrosion rate and the yield strength, ultimate strength and ductility of the corroded steel bars were obtained by data fitting. The obtained models were then compared to the collected experimental data. Generally, good agreement is found between the proposed model and the collected experimental data.

2. Model description

2.1. Analytical model

Consider a corroded steel bar undergoing a tensile test with the applied force F, as shown in Fig. 1. Since the shape is irregular, the elongation rate along the steel bar might not be uniform. It is necessary to determine the elongation rate of the steel bar at each position x.

For a given load F, the average stress on a particular section of steel bar $\sigma(x)$ can be calculated as follows if the cross-sectional area is known:

$$\sigma(x) = \frac{F}{s(x)} \tag{1}$$

where $s(x)$ is the cross-sectional area at position x. Suppose that the area varies very little in the interval $[x, x + dx]$; then, the elongation length dl of this small portion of steel bar can be expressed as:

$$dl(x) = \varepsilon(x)dx \tag{2}$$

where $\varepsilon(x)$ represents the local strain at position x. Then, the elongation of the whole steel bar ΔL can be obtained by integration of the elongation length of each small portion of the steel bar as follows:

$$\Delta L = \int_0^L dl(x) = \int_0^L \varepsilon(x)dx \tag{3}$$

Since the remaining material has the same properties as the original steel material, the tensile constitutive properties remain the same. For every section, there exists a function ζ linking the strain of the material to the stress as follows:

$$\sigma(x) = \zeta(\varepsilon(x)) \tag{4}$$

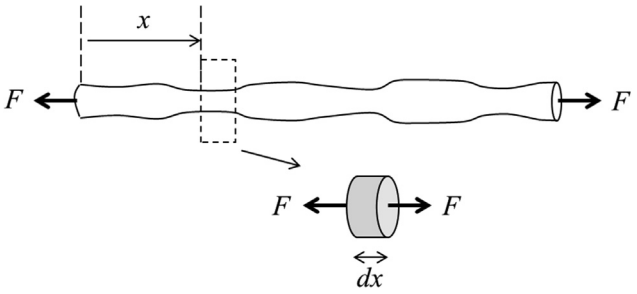

Fig. 1. Corroded steel bar undergoing a uniaxial tensile test.

The function ζ can be obtained by conducting a tensile test on the uncorroded steel bar or by conducting a tensile test on a uniform sample having the same material properties as the corroded steel bar. For construction steels, the function $\zeta$is a monotonically increasing function. Therefore, an inverse function φ of ζexists as follows:

$$\varepsilon(x) = \zeta^{-1}(\sigma(x)) = \varphi(\sigma(x)) \tag{5}$$

In other words, the function φ allows us to find the elongation rate $\varepsilon(x)$ of each section when the stress of the section is known. The shape of the function φ can be obtained by simply rotating the graph of function ζ by 90 degrees in a counter-clockwise orientation, as shown in Fig. 2. By combining equations (1), (3) and (5), one can obtain the following:

$$\Delta L = \int_0^L \varphi(\sigma(x))dx = \int_0^L \varphi\left(\frac{F}{s(x)}\right)dx \tag{6}$$

The section area $s(x)$ of the steel bar can be obtained by an experimental method such as 3D optical scanning or X-ray tomography. For a given load F, the total elongation of the whole corroded steel bar can be calculated using equation (6).

In the above model, the cross-section area $s(x)$ is supposed to be independent of the applied stress. This assumption leads to an underestimation of the stress when the deformation becomes large [29]. It is also interesting to point out that the inverse function of ζ exists if and only if ζ is a monotonically increasing function. For some mild steel bars where a plastic deformation leads to a constant stress or even a small drop in the stress when the strain increases, this process is illustrated in Fig. 3. In such cases, to ensure the existence of a functionφ, a small correction of the function ζ needs to be performed by artificially adding a very small increase in the stress when the strain increases during plastic deformation. This correction is artificial and has very little effect on the quality of the presented model. It is also important to point out that for low carbon steel where necking occurs before fracture, the stress decreases with increasing strain after the maximum stress point. In such cases, the model uses the failure criteria at the maximum stress point instead of the fracture point of the steel material. This treatment slightly underestimates the ultimate strain of the corroded steel bar within a reasonable range [26].

2.2. Numerical implementation

The numerical implementation of the proposed model requires knowledge of the original stress–strain relationship of the uncorroded steel material. Then, the geometric configuration of the corroded steel bar should be measured before the start of the numerical calculation. For a given corroded steel bar with known shape and tensile properties, the above numerical calculation

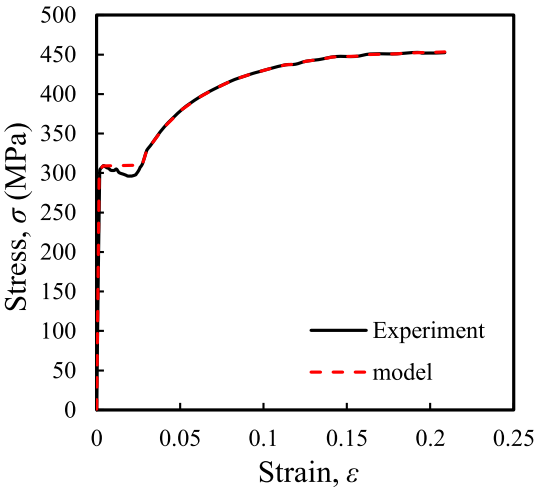

Fig. 3. Adapted numerical model after adjustment of the experimental behaviour for an HPB300 construction steel bar.

allows prediction of the tensile behaviour of the corroded steel bar by following the scheme illustrated in Fig. 4. First, the original stress–strain function ζ is entered. It allows the computation of the inverse functionφ. In the next step, either the 3D profile of the corroded steel bar or the distribution function of the cross-sectional area is required. The program calculates the strain rate of each section of the corroded steel bar. The total elongation length of the corroded steel bar can be obtained by summing the elongation of each section. The procedure ends if any section reaches the maximum allowed stress of the steel material. Then, the total displacement is defined as the sum of the elongation of each section along the corroded steel bar.

3. Experimental validation

A *MATLAB* program was written to validate the above analytical model. Numerical predictions of the tensile behaviour of two series of steel bars were compared to experimentally obtained uniaxial tensile test results. The first series consisted of slotted steel bars that simulated ideal cases of steel corrosion [26]; the second series consisted of electrochemically corroded steel bars [17]. Since in corroded specimens the cross section area is no more uniform due to pitting corrosion, the experimental and numerical results are shown with load–displacement curve instead of stress–strain curve where a uniform cross section area is required. This choice is also made in order to avoid confusion with the material properties presented in Fig. 3.

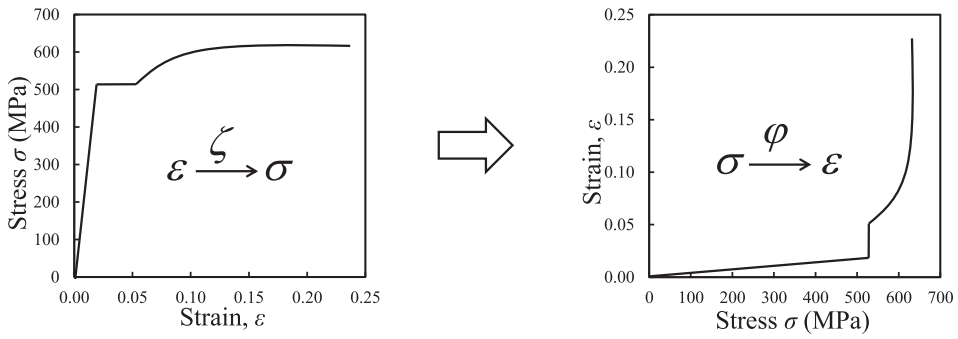

Fig. 2. Illustration of the typical stress–strain behaviour of a steel bar and its inverse function φ.

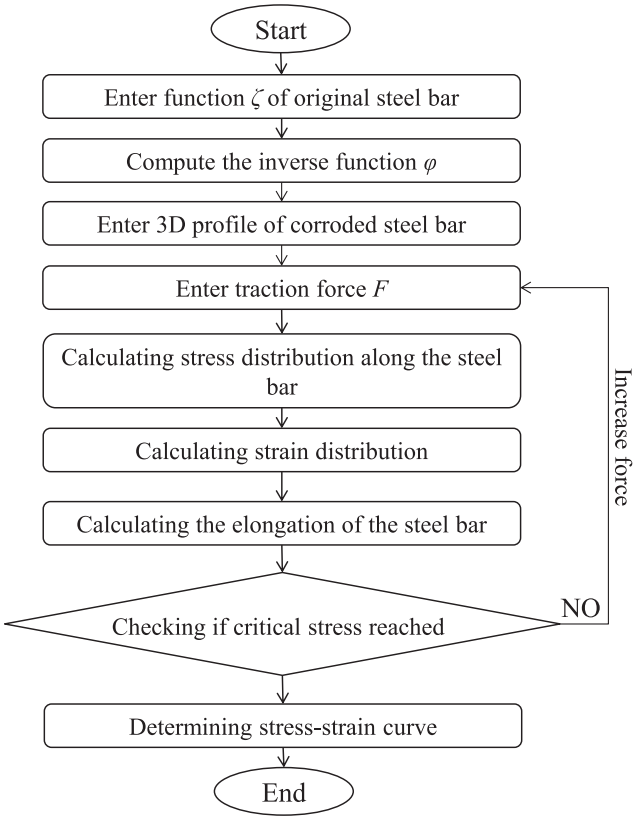

Fig. 4. Numerical scheme for calculation of the stress–strain behaviour of a randomly shaped corroded steel bar.

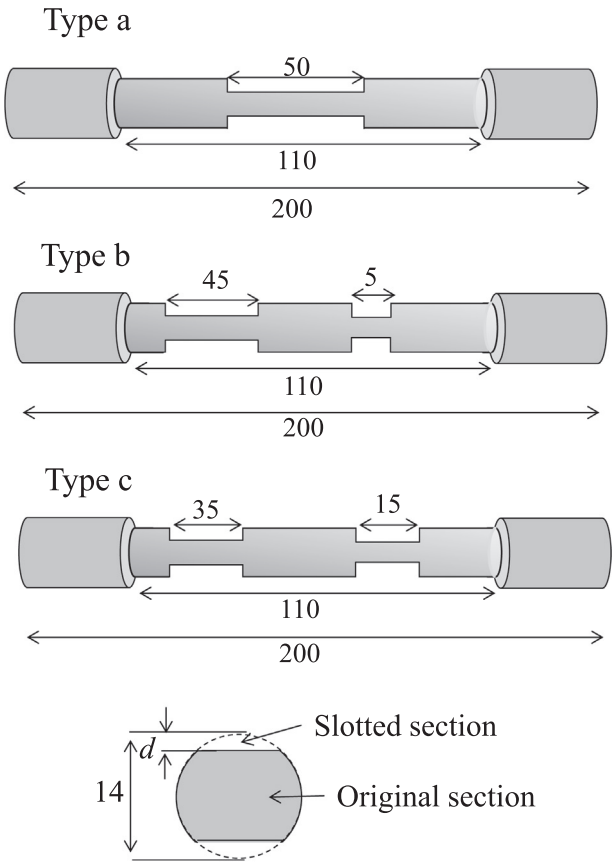

Fig. 5. Geometric configurations of slotted steel bars.

3.1. Comparison with slotted steel bars

The model was compared to slotted steel bars used to simulate artificial corrosion. The detailed experimental program can be found in Li's paper [26]; here, only a brief review of some of the important parameters is given. Ten sets of slotted steel bars were prepared using machine grooving. Each set had three identical specimens. The original diameter of the steel bars was 14 mm, made from HPB300 steel. The length and shape of the slotted section are shown in Fig. 5. Three types of slotted steel bars with different slot depths were prepared to simulate different degrees of corrosion. Uniaxial tensile tests were conducted using a universal tensile test machine.

The slot length and depth are listed in Table 1. The experimental results and the predicted load–displacement curves are shown in Fig. 6. Numerical computations were performed based on the geometric data and the stress–strain relationships of the sound bars. Table 2 lists the experimental results and predicted values for the yield load, ultimate load and displacement at failure and shows that the agreement is reasonable for all three parameters. The model slightly underestimated the displacement at failure of the slotted steel bars in most cases. This is because the model uses the failure criterion at the maximum stress point of the steel material instead of the fracture point. In the experiments, a small drop in the load was observed after the maximum stress was reached in the smallest section; therefore, the measured displacement was slightly higher than the predicted values. However, the relative errors of the numerical predictions were all smaller than 10%. For the ultimate load and yield load, the agreement between the analytical model and experimental results was rather good. The relative errors were all smaller than 4%. On the one hand, this is because the analytical model focuses particularly on the maximum stress point; on the other hand, these results prove that the maximum load of a corroded steel bar is controlled by the minimum cross-sectional area of the corroded steel bar, as reported by several other authors [1–3]. The results presented in this section prove the ability of the analytical model to predict the tensile behaviour of slotted steel bars.

Table 1
Parameters of the slotted steel bars.

Set	Slot length $l/[l_1, l_2]$ (mm)	Slot depth d (mm)
S-2-a	50	2.56
S-2-b	[45,5]	2.56
S-2-c	[35,15]	2.56
S-4-a	50	4.17
S-4-b	[45,5]	4.17
S-4-c	[35,15]	4.17
S-5-a	50	5.62
S-5-b	[45,5]	5.62
S-5-c	[35,15]	5.62

3.2. Comparison with electrochemically corroded steel bars

To verify the validity of the analytical model, it would also be interesting to compare the results of the analytical model with experiments on accelerated corroded steel bars. Accelerated corrosion is a widely used method to obtain a sufficient degree of corrosion in a relatively short time [16–19]. However, it is interesting to point out that, electrical fields in accelerated laboratory corrosion tests would change the corrosion process. A novel method gives

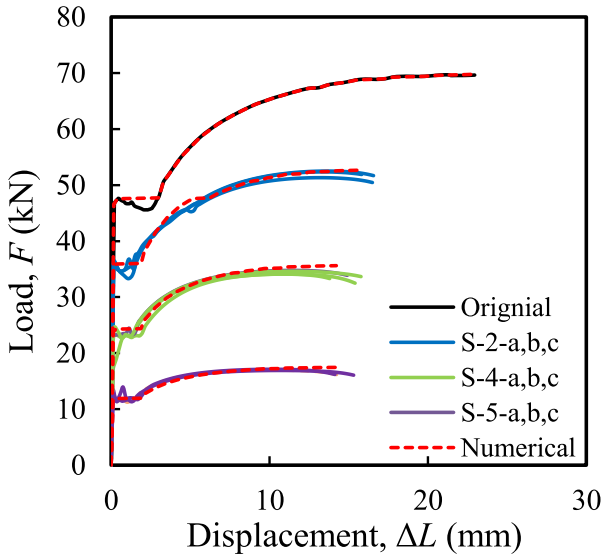

Fig. 6. Comparison between the experimental results of slotted rebars and numerical results.

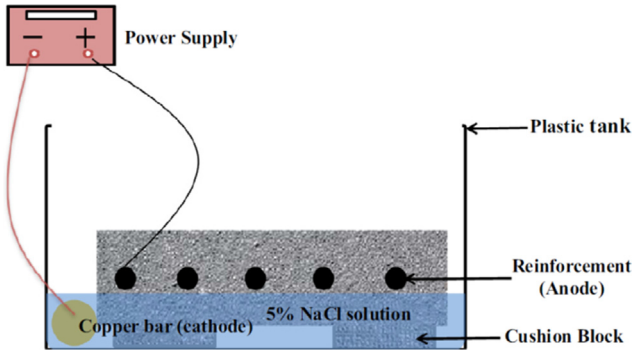

Fig. 7. Accelerated corrosion test for HPB400 construction steel specimens.

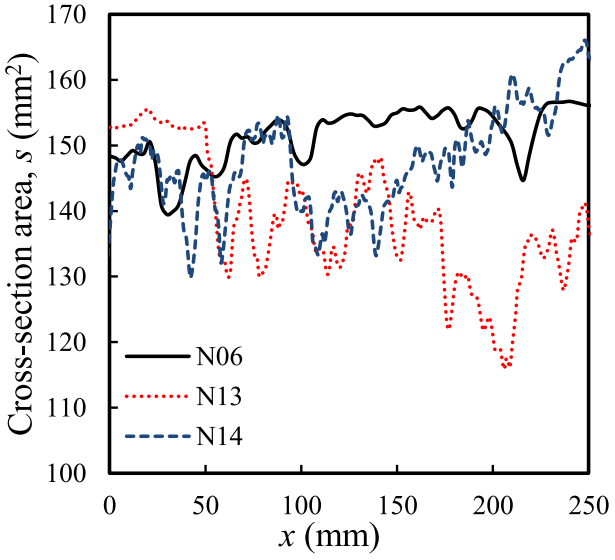

Fig. 8. Typical scanning profile of the corroded steel bars.

link from accelerated test to the time scale of the chloride ingress without electric field through Arrhenius-type considerations [31].

Nine electrochemically corroded steel bars of type HPB400 were prepared by accelerated corrosion tests using direct current, as shown in Fig. 7. The diameter of the steel bars is 14 mm, and the length is 250 mm. The detailed experimental program was described in [17]. After the accelerated corrosion tests, the steel bars were cleaned using the standard method specified in ASTM G1-03 [30]. The geometric configurations of the clean corroded steel bars were measured by 3D light scanning. The accuracy of the scanning method was 0.5 mm in length and 1 degree in the angle. Typical scanning results are shown in Fig. 8. The degree of corrosion measured by means of sectional area method ranged from 3.2% to 15%. Using the obtained geometric configurations, the tensile behaviour of the corroded steel bars was predicted by the proposed analytical model. Uniaxial tensile tests of the corroded steel bars were performed to confirm the validity of the obtained results.

Fig. 9 displays comparisons between the predicted behaviour by the analytical model and the experimental results for three typical corroded steel bars. For corroded specimens, the yielding force could not be determined by yielding platform. Therefore, in this paper the yielding forces are determined as the end of the linear part on a load–displacement curve. Numerically, it is determined by the force where a sharp decrease of the linear slope was observed. This force corresponds to the yielding force for the smallest section of the corroded specimens. It could be seen from Fig. 9 that the analytical model could predict the tensile behaviour of the corroded steel bars with satisfactory accuracy. Table 3 lists the experimental results and numerical predictions for the yield load F_y, ultimate load F_u and displacement at failure ΔL_f and shows that

Table 2
Comparison between the numerical results and experimental results for slotted steel bars.

Specimen	Yield load, F_y (kN)			Ultimate load, F_u (kN)			Displacement at failure, ΔL_f (mm)		
	Exp	Num	Ratio	Exp	Num	Ratio	Exp	Num	Ratio
S-2-a	47.7	47.7	1.00	69.7	69.7	1.00	16.3	15.6	1.04
S-2-b	35.9	36.0	1.01	51.3	52.7	0.97	15.8	15.6	1.01
S-2-c	36.5	36.0	1.01	52.7	52.7	1.00	15.6	15.6	1.00
S-4-a	36.3	36.0	1.01	52.4	52.7	0.99	15.1	14.2	1.06
S-4-b	24.6	24.3	0.96	34.8	35.6	0.98	13.6	14.2	0.96
S-4-c	23.2	24.3	0.95	34.6	35.6	0.97	14.5	14.2	1.02
S-5-a	23.1	24.3	1.00	34.1	35.6	0.96	14.9	14.2	1.05
S-5-b	11.9	11.9	1.01	16.9	17.5	0.97	15.0	14.2	1.05
S-5-c	13.5	11.9	1.14	17.1	17.5	0.98	14.7	14.2	1.04
Cov	\	\	1.01	\	\	0.98	\	\	1.03
Std	\	\	0.05	\	\	0.01	\	\	0.03

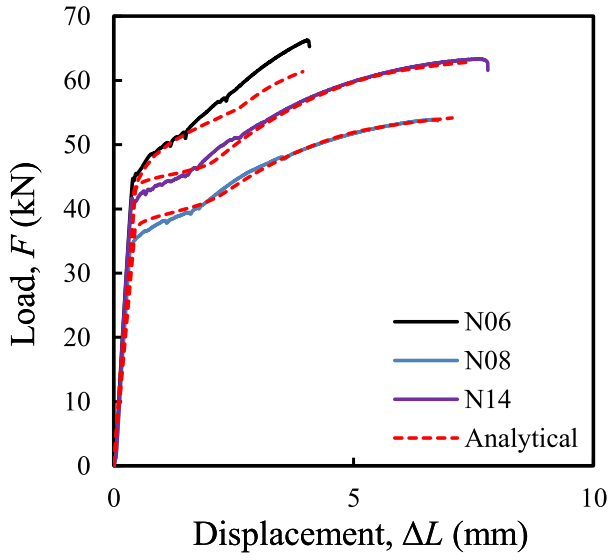

Fig. 9. Predicted tensile behaviour compared to experimental results for three electrochemically corroded steel bars.

the analytical model slightly underestimated the ultimate load and displacement at failure but overestimated the yield load. Although some large deviations could be observed for specimens N09 and N10, the general predictions were good enough with errors smaller than 10% on average. These results further confirmed the validity of the proposed analytical model.

4. Prediction of the tensile behaviour of corroded steel bars based on a log-normal distribution

The above analysis validated the proposed analytical model. It would then be interesting to investigate the effect of corrosion on the tensile behaviour of a randomly corroded steel bar. The important parameters for defining a constitutive model of a corroded steel bar are the yield strength, the ultimate strength and the ductility. In the following sections, these parameters were studied for numerically generated corroded steel bars using the proposed analytical model.

4.1. Numerical generation of corroded steel bars

For steel bars corroded in high-chloride environments, the typical corrosion mode is pitting corrosion [20–23]. The most common form of the distribution of the cross-sectional area of a corroded steel bar is a log-normal distribution as follows [19,20]:

$$f(s|\mu,m)=\frac{1}{sm\sqrt{2\pi}}\exp\left(\frac{-(\ln s-\mu)^2}{2m^2}\right) \tag{7}$$

where μ and m are the parameters of the log-normal distribution. Kashani et al. performed optical scanning on corroded steel bars [19]. They found that these two parameters followed power laws with the corrosion rate w (which was defined as the average cross-section loss) as follows:

$$\mu=-0.00052\cdot w^{1.825} \tag{8}$$

$$m=0.0006491\cdot w^{1.526} \tag{9}$$

Hence, in the following, we assumed that the corroded sections follow a log-normal distribution and that the parameters of the log-normal distribution follow the power laws given by equations (8) and (9). Based on these assumptions, Monte-Carlo simulations were performed to numerically generate corroded steel bars. The generation process started by randomly choosing a value of corrosion rate between 0 and 60%. Then, the two parameters of the log-normal distribution could be determined using equations (8) and (9), and the distribution of the cross-sectional area was uniquely defined. For the numerically generated corroded steel bars, the input stress–strain relation followed that of type HPB400 steel. The length was supposed to be 300 mm and was equally divided into 600 segments. For each segment, the surface area was generated using a random function with a log-normal distribution. This treatment guaranteed the final distribution of the surface area. Fig. 10 gives an example of the surface areas of randomly generated corroded steel bars with different corrosion rates w.

It is interesting to point out that the generated model is much rougher than the scanned profile. This is because in reality, the wideness of a pit hole is proportional to the pit depth. If high corrosion happens in a location, it is highly possible that within its neighbourhood, the local corrosion rate is also high. However, this effect was not considered during the numerical generation process. The numerical generation process focused only on the final distribution of the sectional area, and the order of small and large local corrosion was ignored. In the analytical model, this effect does not play any role. Therefore, the calculated load–displacement profile is unaffected.

Using the algorithm given in Fig. 4, the load–displacement behaviours of the numerically generated corroded steel bars were computed. Typical results are illustrated in Fig. 11. The following parameters are defined to characterise the tensile behaviour of a generated corroded steel bar based on its load–displacement curve. The relative yield strength σ_y is defined as the load F_y at the end of

Table 3
Comparison between the numerical results and experimental results for electrochemically corroded steel bars.

Specimen	Corrosion degree, w (%)	Yield load, F_y (kN)			Ultimate load, F_u (kN)			Displacement at failure, ΔL_f (mm)		
		Exp	Num	Ratio	Exp	Num	Ratio	Exp	Num	Ratio
N06	3.3	42.37	41.59	1.02	64.41	59.78	1.08	3.53	2.93	1.21
N07	13.7	30.98	31.11	1.00	45.50	46.17	0.99	2.63	3.23	0.81
N08	14.1	33.13	35.65	0.93	52.42	52.76	0.99	5.78	5.10	1.13
N09	12.1	40.13	44.04	0.91	70.17	60.41	1.16	3.53	2.93	1.21
N10	13.9	38.50	32.63	1.18	56.68	46.28	1.22	1.35	1.20	1.13
N11	12.3	40.19	39.72	1.01	65.07	60.41	1.08	4.05	3.68	1.10
N12	11.4	39.72	43.91	0.90	63.62	61.87	1.03	3.23	3.53	0.91
N13	15.1	37.10	40.23	0.92	57.87	55.85	1.04	4.43	3.83	1.16
N14	8.4	39.73	42.09	0.94	61.56	61.29	1.00	6.53	5.48	1.19
Cov	\	\	\	0.98	\	\	1.07	\	\	1.09
Std	\	\	\	0.09	\	\	0.08	\	\	0.14

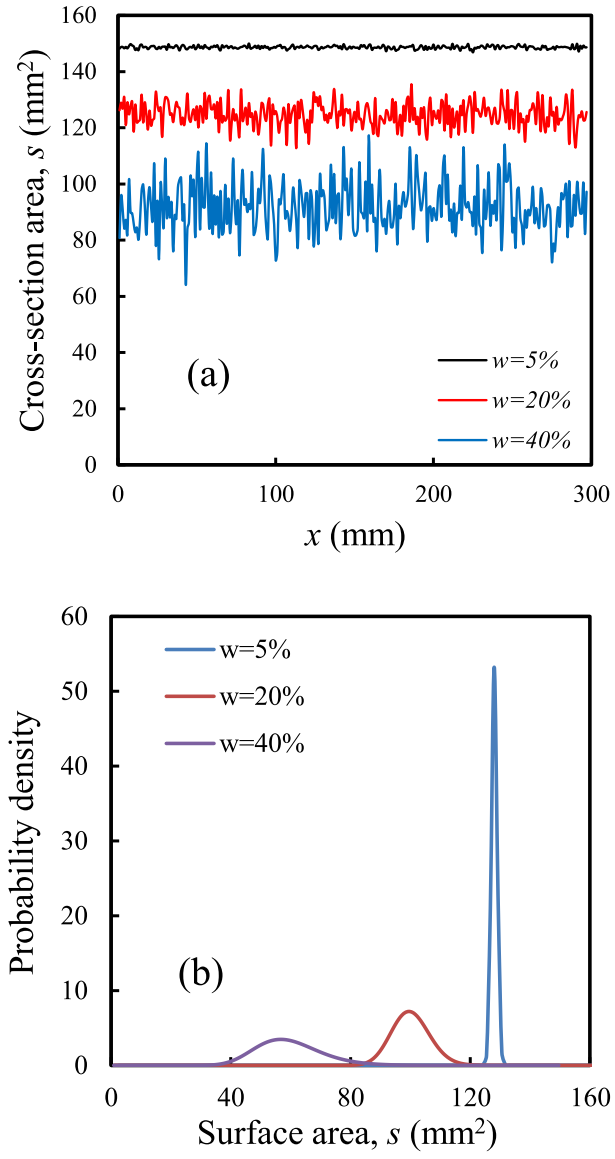

Fig. 10. Numerically generated corroded steel bars and the distribution of the section area.

the linear part of the load–displacement curve divided by the uncorroded yield load F_{y0} as follows:

$$\sigma_y = \frac{F_y}{F_{y0}} \tag{10}$$

The relative ultimate strength σ_u is defined as the maximum load $F_{\max}$ divided by the maximum load of the uncorroded steel bar $F_{\max 0}$ as follows:

$$\sigma_u = \frac{F_{\max}}{F_{\max 0}} \tag{11}$$

The relative ductility ε_u is defined as the displacement at failure ΔL_f divided by the displacement at failure for the uncorroded steel bar ΔL_{f0} as follows:

$$\varepsilon_u = \frac{\Delta L_f}{\Delta L_{f0}} \tag{12}$$

These parameters are defined to avoid confusion in the following discussion.

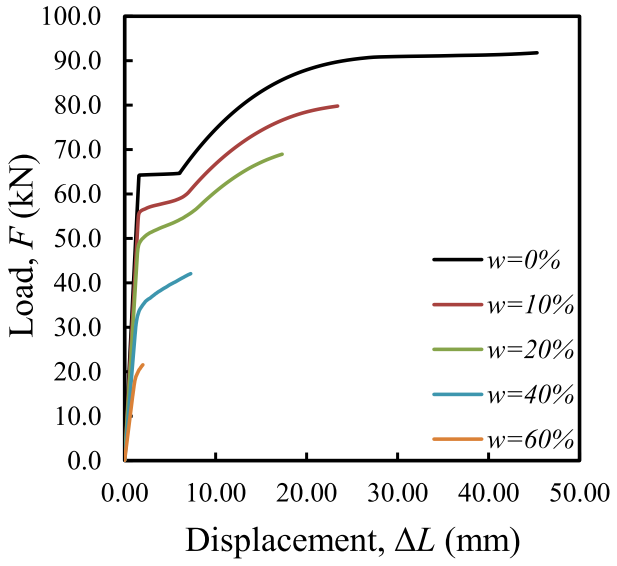

Fig. 11. Typical load–displacement curve of the numerically generated corroded steel bars.

4.2. Effect of corrosion on the yield and ultimate strength of a corroded steel bar

For each generated corroded steel bar, the relative yield and ultimate strengths were identified, and the results are plotted according to the average corrosion rate w, as shown in Fig. 12. This figure shows that the relative yield and ultimate strengths exhibit linear decreases with increasing corrosion rate. The following equations are the result of linear fitting of the numerical results:

$$\sigma_y = 1 - 0.0126w \tag{13}$$

$$\sigma_u = 1 - 0.0129w \tag{14}$$

These numerical results agree well with the experimental results observed by several authors. Sun et al. summarised existing empirical models for the strength prediction of corroded steel bars for both naturally corroded steel bars and electrochemically accelerated corroded steel bars [18]. All authors proposed linear models for both yield strength and ultimate strength. For relative yield strength, the linear factor ranges from 0.0072 to 0.0210, with an average of 0.0132. For ultimate strength, the linear factor ranges between 0.0086 and 0.0231, with an average of 0.0145. Both values are very close to the obtained results for the numerically generated corroded steel bars. Fig. 13 displays a comparison of the predicted yield and ultimate strength obtained using equations (13) and (14) with available experimental raw data and shows that the models agree well with the experimental results.

4.3. Effect of corrosion on the ductility of corroded steel bars

The deformation capacity of corroded steel bars is another important parameter since it directly affects the ductility of reinforced concrete members. Numerous experimental results have shown that the ultimate strain decreases with corrosion rate. It would be interesting to determine the parameters that control the ductility of corroded steel bars. To find a unified relationship between the corrosion rate and the ductility of corroded steel bars, 300 corroded steel bars were generated using a log-normal distribution for the corroded section with various degrees of corrosion.

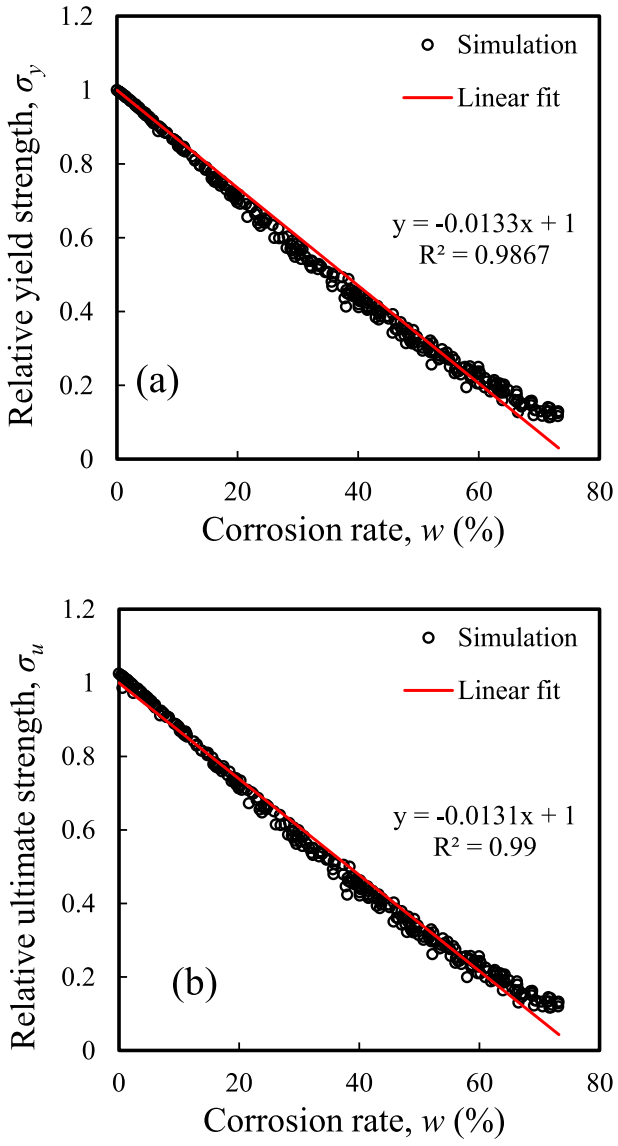

Fig. 12. Relationship between relative yield strength (a) and relative ultimate strength (b) with corrosion rate.

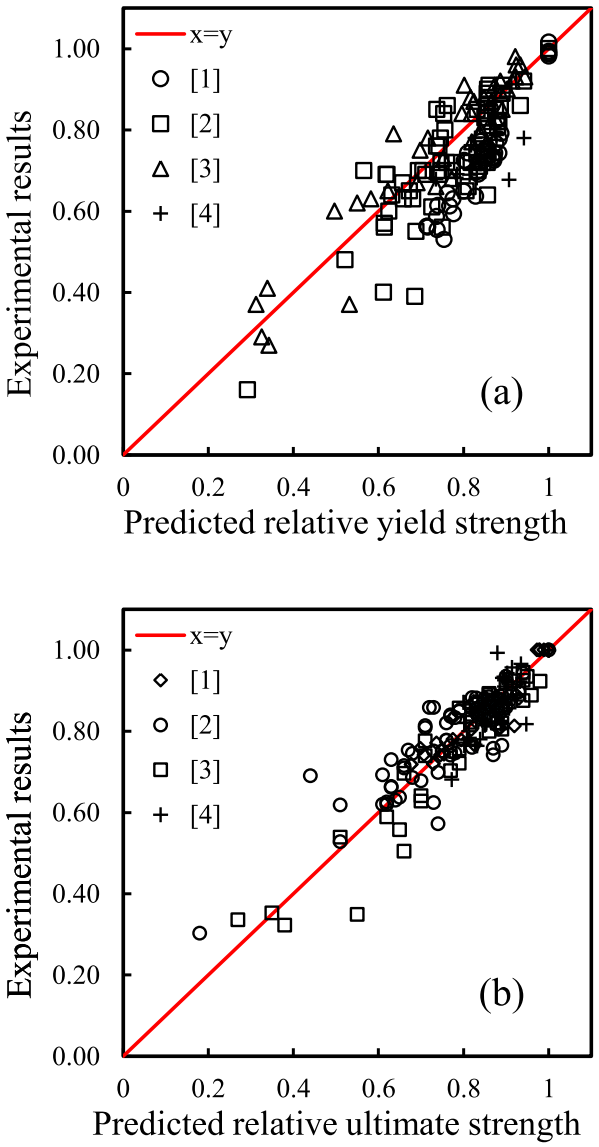

Fig. 13. Comparison of the predicted relative ultimate strength with the experimental results for relative yield strength (a) and relative ultimate strength (b). Experimental results were provided by Moreno et al. [1], Imperatore et al. [2], Fernandez et al. [3] and Ou et al. [4].

The ductility of the corroded steel bars was calculated using equation (12) for different corrosion rates.

Fig. 14 displays the relationship between the relative ductility ε_u and the corrosion rate w for the numerically generated corroded steel bars. There is an exponential decrease in the ductility with the corrosion rate. The following equation is the result of data fitting of the numerically generated corroded steel bars:

$$\varepsilon_u = e^{-0.061w} \tag{15}$$

This exponential decrease could be explained by the fact that with increasing corrosion, the spectrum of the distribution of the corroded section becomes larger. Indeed, since the cross-section of the corroded steel bars was assumed to follow a log-normal distribution, the failure criteria were defined when the maximum stress was reached in the smallest cross-section area. Hence, when the smallest cross-section reaches its maximum stress level, the part that undergoes plastic deformation and strain hardening decreases exponentially since the distribution function is a log-normal function. Therefore, the relative ductility decreases exponentially with the corrosion rate. Fig. 15 displays the strain distribution of the corroded steel bars in the critical state and shows that for a small corrosion rate (w = 5%, 10% and 15%), the deformation of the segments is large, nearly all entering the strain-hardening range. For a high corrosion rate (w = 30%), only a small portion of the segments enters the strain-hardening stage. Most of the deformation was smaller than 0.04, signifying elastic and plastic deformation. Therefore, the exponential decrease in the ductility is strongly related to the heterogeneity of the deformation of the corroded section in the critical state.

The rapid decrease in ductility with increasing corrosion was also observed in numerous experimental results [1–3]. Fig. 16 displays a comparison of the predicted ductility using equation (15) with the experimental results and shows that the prediction is conservative compared to the experimental results. This is because the analytical model uses the failure criteria at the maximum stress level, thus underestimating the final strain at the fracture of the steel bar. Another possible source of underestimation could be the effect of the distribution of the corroded sec-

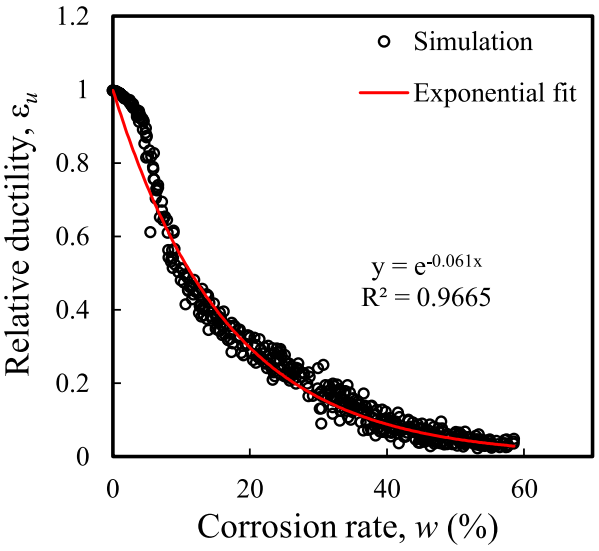

Fig. 14. Relative ductility for numerically generated corroded steel bars.

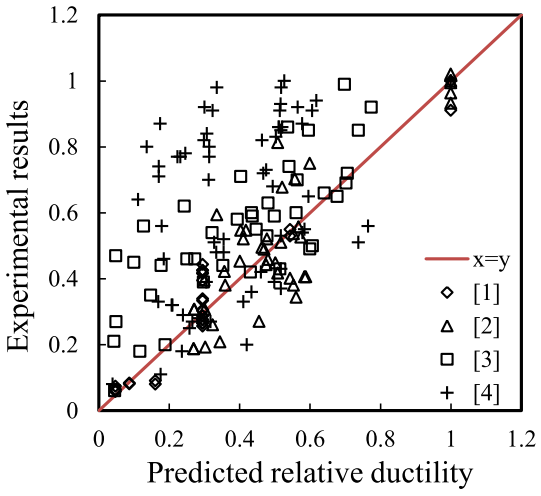

Fig. 16. Comparison of the predicted relative ductility with the experimental results. Experimental results were provided by Moreno et al. [1], Imperatore et al. [2], Fernandez et al. [3] and Ou et al. [4].

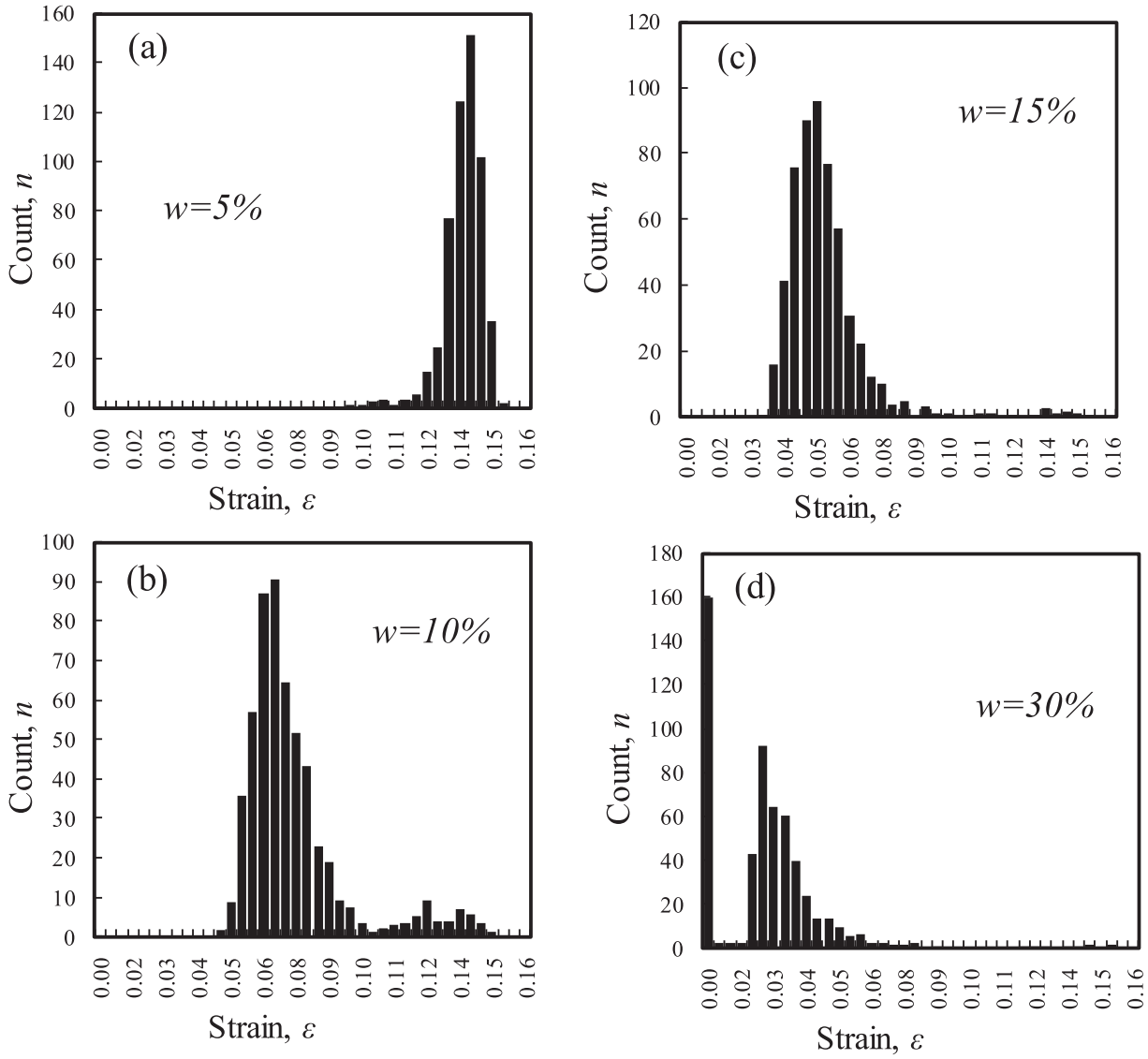

Fig. 15. Distribution of the strain at failure for different corrosion rates.

tions. Indeed, equation (15) is obtained by assuming a log-normal distribution of the corroded section. This assumption might not be true in many cases. For experiments conducted by Ou et al. with naturally corroded steel bars, high ductility was observed even for highly corroded steel bars [4]. This is because corrosion in the natural environment might be the result of several factors, including chloride attack and carbonation of concrete materials. Carbonation-induced corrosion is more homogeneous. In this case, the corroded section does not follow a log-normal distribution. If the section reduction is uniform along the corroded steel bar, then the yielding and fracture occur simultaneously in any section of the steel bar. The ductility of the corroded steel bar remains unchanged. More information on the statistics of the corroded section needs to be given to generate a more reliable model regarding ductility.

5. Conclusions

An analytical model was developed to predict the tensile behaviour of a corroded steel bar based on cross-sectional analysis. The model was implemented in *MATLAB*, and the numerical results were validated by slotted steel bars and electrochemically corroded steel bars. Based on a log-normal distribution of the corroded section, the tensile behaviour of corroded steel bars was predicted using the proposed analytical model. The following conclusions can be drawn:

1. The proposed analytical model can give good predictions of the tensile behaviour of the slotted steel bars and electrochemically corroded steel bars, provided the profile of the section area is known;
2. Predictions of the tensile behaviour of corroded steel bars were made based on a log-normal distribution function and Monte-Carlo simulations. The simulation results showed that relative yield and ultimate strength decreased linearly with the increasing corrosion rate. Numerical models were proposed by data fitting. Compared to the experimental data collected by various authors, the proposed models give good predictions of the decreases in the yield and ultimate strength of corroded steel bars.
3. A rapid decrease in the ductility of corroded steel bars was observed using a log-normal distribution of the corroded cross-sections. An exponential decrease model was given by data fitting. Compared to the collected experimental data, the proposed model is generally conservative.

CRediT authorship contribution statement

Chaoqun Zeng: Investigation, Methodology, Formal analysis, Writing - original draft. **Ji-Hua Zhu:** Writing - review & editing, Supervision, Funding acquisition. **Cheng Xiong:** . **Yanru Li:** Writing - review & editing. **Dawang Li:** Methodology. **Joost Walraven:** Writing - review & editing.

Declaration of Competing Interest

The authors declare that they have no known competing financial interests or personal relationships that could have appeared to influence the work reported in this paper.

Acknowledgements

The research described in this paper was supported by the Key-Area Research and Development Program of Guangdong Province (2019B111107002), the National Key Research and Development Program of China (2018YFE0124900), the National Natural Science Foundation of China (51538007/51778370/51861165204/1520105012 and 51978406), the Natural Science Foundation of Guangdong (2017B030311004), and the Shenzhen Science and Technology Project (GJHZ20180928155819738).

References

[1] E. Moreno, A. Cobo, G. Palomo, M.N. González, Mathematical models to predict the mechanical behavior of reinforcements depending on their degree of corrosion and the diameter of the rebars, Constr. Build. Mater. 61 (2014) 156–163, https://doi.org/10.1016/j.conbuildmat.2014.03.003.
[2] S. Imperatore, Z. Rinaldi, C. Drago, Degradation relationships for the mechanical properties of corroded steel rebars, Constr. Build. Mater. 148 (2017) 219–230, https://doi.org/10.1016/j.conbuildmat.2017.04.209.
[3] I. Fernandez, J.M. Bairán, A.R. Marí, Corrosion effects on the mechanical properties of reinforcing steel bars. Fatigue and σ–ε behavior, Constr. Build. Mater. 101 (2015) 772–783, https://doi.org/10.1016/j.conbuildmat.2015.10.139.
[4] Y.-C. Ou, Y.T.T. Susanto, H. Roh, Tensile behavior of naturally and artificially corroded steel bars, Constr. Build. Mater. 103 (2016) 93–104, https://doi.org/10.1016/j.conbuildmat.2015.10.075.
[5] W. Zhu, R. François, C.S. Poon, J.-G. Dai, Influences of corrosion degree and corrosion morphology on the ductility of steel reinforcement, Constr. Build. Mater. 148 (2017) 297–306, https://doi.org/10.1016/j.conbuildmat.2017.05.079.
[6] J. Chen, Y. Zhao, L. Wu, W. Jin, Experimental investigation and design of corroded stud shear connectors, Adv. Struct. Eng. 19 (2) (2016) 218–226, https://doi.org/10.1177/1369433215624327.
[7] W. P. Zhang, D.F. Shang, X.L. Gu, Stress-strain relationship of corroded steel bars, J. Tongji Univ. (Nat. Sci.) 34 (5) (2006) 586–592 (in Chinese).
[8] D. Coronelli, P. Gambarova, Structural Assessment of Corroded Reinforced Concrete Beams: Modeling Guidelines, J. Struct. Eng. 130 (8) (2004) 1214–1224, https://doi.org/10.1061/(ASCE)0733-9445(2004)130:8(1214).
[9] M. Otieno, H. Beushausen, M. Alexander, Chloride-induced corrosion of steel in cracked concrete – Part I: Experimental studies under accelerated and natural marine environments, Cem. Concr. Res. 79 (2016) 373–385, https://doi.org/10.1016/j.cemconres.2015.08.009.
[10] M. Otieno, H. Beushausen, M. Alexander, Chloride-induced corrosion of steel in cracked concrete—Part II: Corrosion rate prediction models, Cem. Concr. Res. 79 (2016) 386–394, https://doi.org/10.1016/j.cemconres.2015.08.008.
[11] S. Laurens, P. Hénocq, N. Rouleau, F. Deby, E. Samson, J. Marchand, B. Bissonnette, Steady-state polarization response of chloride-induced macrocell corrosion systems in steel reinforced concrete — numerical and experimental investigations, Cem. Concr. Res. 79 (2016) 272–290, https://doi.org/10.1016/j.cemconres.2015.09.021.
[12] C. Andrade, C. Alonso, J. Gulikers, R. Polder, R. Cigna, O. Vennesland, M. Salta, A. Raharinaivo, B. Elsener, Test methods for on-site corrosion rate measurement of steel reinforcement in concrete by means of the polarization resistance method, Mater. Struct. 37 (273) (2004) 623–643, https://doi.org/10.1007/BF02483292.
[13] A. Goyal, H.S. Pouya, E. Ganjian, A.O. Olubanwo, M. Khorami, Predicting the corrosion rate of steel in cathodically protected concrete using potential shift, Constr. Build. Mater. 194 (2019) 344–349, https://doi.org/10.1016/j.conbuildmat.2018.10.153.
[14] X. Xi, S. Yang, Investigating the spatial development of corrosion of corner-located steel bar in concrete by X-ray computed tomography, Constr. Build. Mater. 221 (2019) 177–189, https://doi.org/10.1016/j.conbuildmat.2019.06.023.
[15] S. Hong, H. Wiggenhauser, R. Helmerich, B. Dong, P. Dong, F. Xing, Long-term monitoring of reinforcement corrosion in concrete using ground penetrating radar, Corros. Sci. 114 (2017) 123–132, https://doi.org/10.1016/j.corsci.2016.11.003.
[16] D. Li, R. Wei, Y. Du, X. Guan, M. Zhou, Measurement methods of geometrical parameters and amount of corrosion of steel bar, Constr. Build. Mater. 154 (2017) 921–927, https://doi.org/10.1016/j.conbuildmat.2017.08.018.
[17] D. Li, R. Wei, L. Li, X. Guan, X. Mi, Pitting corrosion of reinforcing steel bars in chloride contaminated concrete, Constr. Build. Mater. 199 (2019) 359–368, https://doi.org/10.1016/j.conbuildmat.2018.12.003.
[18] X. Sun, H. Kong, H. Wang, Z. Zhang, Evaluation of corrosion characteristics and corrosion effects on the mechanical properties of reinforcing steel bars based on three-dimensional scanning, Corros. Sci. 142 (2018) 284–294, https://doi.org/10.1016/j.corsci.2018.07.030.
[19] M.M. Kashani, A.J. Crewe, N.A. Alexander, Use of a 3D optical measurement technique for stochastic corrosion pattern analysis of reinforcing bars subjected to accelerated corrosion, Corros. Sci. 73 (2013) 208–221, https://doi.org/10.1016/j.corsci.2013.03.037.
[20] F. Caleyo, J.C. Velázquez, A. Valor, J.M. Hallen, Probability distribution of pitting corrosion depth and rate in underground pipelines: A Monte Carlo study, Corros. Sci. 51 (9) (2009) 1925–1934, https://doi.org/10.1016/j.corsci.2009.05.019.
[21] G. Qian, M. Niffenegger, S. Li, Probabilistic analysis of pipelines with corrosion defects by using FITNET FFS procedure, Corros. Sci. 53 (3) (2011) 855–861, https://doi.org/10.1016/j.corsci.2010.10.014.

[22] J.A. González, C. Andrade, C. Alonso, S. Feliu, Comparison of rates of general corrosion and maximum pitting penetration on concrete embedded steel reinforcement, Cem. Concr. Res. 25 (2) (1995) 257–264, https://doi.org/10.1016/0008-8846(95)00006-2.
[23] Y. Zhao, X. Zhang, H. Ding, W. Jin, Non-uniform distribution of a corrosion layer at a steel/concrete interface described by a Gaussian model, Corros. Sci. 112 (2016) 1–12, https://doi.org/10.1016/j.corsci.2016.06.021.
[24] D. Rivas, F. Caleyo, A. Valor, J.M. Hallen, Extreme value analysis applied to pitting corrosion experiments in low carbon steel: comparison of block maxima and peak over threshold approaches, Corros. Sci. 50 (11) (2008) 3193–3204, https://doi.org/10.1016/j.corsci.2008.08.002.
[25] F. Tang, Z. Lin, G. Chen, W. Yi, Three-dimensional corrosion pit measurement and statistical mechanical degradation analysis of deformed steel bars subjected to accelerated corrosion, Constr. Build. Mater. 70 (2014) 104–117, https://doi.org/10.1016/j.conbuildmat.2014.08.001.
[26] D. Li, C. Xiong, T. Huang, R. Wei, N. Han, F. Xing, A simplified constitutive model for corroded steel bars, Constr. Build. Mater. 186 (2018) 11–19, https://doi.org/10.1016/j.conbuildmat.2018.07.019.
[27] I. Fernandez, J.M. Bairán, A.R. Marí, 3D FEM model development from 3D optical measurement technique applied to corroded steel bars, Constr. Build. Mater. 124 (2016) 519–532, https://doi.org/10.1016/j.conbuildmat.2016.07.133.
[28] R. Francois, I. Khan, V.H. Dang, Impact of corrosion on mechanical properties of steel embedded in 27-year-old corroded reinforced concrete beams, Mater. Struct. 46 (6) (2013) 899–910, https://doi.org/10.1617/s11527-012-9941-z.
[29] Y. Garbatov, C. Guedes Soares, J. Parunov, J. Kodvanj, Tensile strength assessment of corroded small scale specimens, Corros. Sci. 85 (2014) 296–303, https://doi.org/10.1016/j.corsci.2014.04.031.
[30] ASTM G1-03(2017)e1, Standard Practice for Preparing, Cleaning, and Evaluating Corrosion Test Specimens, ASTM International, West Conshohocken, PA, 2017, www.astm.org
[31] P. Gideon, P. Suvash Chandra, A novel link of the time scale in accelerated chloride-induced corrosion test in reinforced SHCC, Construction and Building Materials, Volume 167, 2018, Pages 15-19, ISSN 0950-0618, 10.1016/j.conbuildmat.2018.02.019.